Biomedical Optics EXPRESS

Miniature fiber-optic multiphoton microscopy system using frequency-doubled femtosecond Er-doped fiber laser

Lin Huang,[1] Arthur K. Mills,[2] Yuan Zhao,[1] David J. Jones,[2] and Shuo Tang[1,*]

[1]*Department of Electrical and Computer Engineering, University of British Columbia, Vancouver, V6T 1Z4, Canada*
[2]*Department of Physics & Astronomy, University of British Columbia, Vancouver, V6T 1Z4, Canada*
[*]*tang@ece.ubc.ca*

Abstract: We report on a miniature fiber-optic multiphoton microscopy (MPM) system based on a frequency-doubled femtosecond Er-doped fiber laser. The femtosecond pulses from the laser source are delivered to the miniature fiber-optic probe at 1.58 μm wavelength, where a standard single mode fiber is used for delivery without the need of free-space dispersion compensation components. The beam is frequency-doubled inside the probe by a periodically poled MgO:$LiNbO_3$ crystal. Frequency-doubled pulses at 786 nm with a maximum power of 80 mW and a pulsewidth of 150 fs are obtained and applied to excite intrinsic signals from tissues. A MEMS scanner, a miniature objective, and a multimode collection fiber are further used to make the probe compact. The miniature fiber-optic MPM system is highly portable and robust. *Ex vivo* multiphoton imaging of mammalian skins demonstrates the capability of the system in imaging biological tissues. The results show that the miniature fiber-optic MPM system using frequency-doubled femtosecond fiber laser can potentially bring the MPM imaging for clinical applications.

OCIS codes: (170.2150) Endoscopic imaging; (190.4180) Multiphoton processes.

References and links

1. T. G. Oertner, "Functional imaging of single synapses in brain slices," Exp. Physiol. **87**(6), 733–736 (2002).
2. T. Ladewig, P. Kloppenburg, P. M. Lalley, W. R. Zipfel, W. W. Webb, and B. U. Keller, "Spatial profiles of store-dependent calcium release in motoneurones of the nucleus hypoglossus from newborn mouse," J. Physiol. **547**(3), 775–787 (2003).
3. E. B. Brown, R. B. Campbell, Y. Tsuzuki, L. Xu, P. Carmeliet, D. Fukumura, and R. K. Jain, "*In vivo* measurement of gene expression, angiogenesis and physiological function in tumors using multiphoton laser scanning microscopy," Nat. Med. **7**(7), 864–868 (2001).
4. D. M. McDonald and P. L. Choyke, "Imaging of angiogenesis: from microscope to clinic," Nat. Med. **9**(6), 713–725 (2003).
5. W. R. Zipfel, R. M. Williams, and W. W. Webb, "Nonlinear magic: multiphoton microscopy in the biosciences," Nat. Biotechnol. **21**(11), 1369–1377 (2003).
6. F. Helmchen and W. Denk, "Deep tissue two-photon microscopy," Nat. Methods **2**(12), 932–940 (2005).
7. B. A. Flusberg, J. C. Jung, E. D. Cocker, E. P. Anderson, and M. J. Schnitzer, "*In vivo* brain imaging using a portable 3.9 gram two-photon fluorescence microendoscope," Opt. Lett. **30**(17), 2272–2274 (2005).
8. J. Sawinski, D. J. Wallace, D. S. Greenberg, S. Grossmann, W. Denk, and J. N. Kerr, "Visually evoked activity in cortical cells imaged in freely moving animals," Proc. Natl. Acad. Sci. U.S.A. **106**(46), 19557–19562 (2009).
9. S. Tang, W. Jung, D. McCormick, T. Xie, J. Su, Y. C. Ahn, B. J. Tromberg, and Z. Chen, "Design and implementation of fiber-based multiphoton endoscopy with microelectromechanical systems scanning," J. Biomed. Opt. **14**, 034005 (2009).
10. Y. Wu, Y. Leng, J. Xi, and X. Li, "Scanning all-fiber-optic endomicroscopy system for 3D nonlinear optical imaging of biological tissues," Opt. Express **17**(10), 7907–7915 (2009).
11. D. R. Rivera, C. M. Brown, D. G. Ouzounov, I. Pavlova, D. Kobat, W. W. Webb, and C. Xu, "Compact and flexible raster scanning multiphoton endoscope capable of imaging unstained tissue," Proc. Natl. Acad. Sci. U.S.A. **108**(43), 17598–17603 (2011).

#259144 Received 9 Feb 2016; revised 5 Apr 2016; accepted 6 Apr 2016; published 19 Apr 2016

12. C. L. Hoy, O. Ferhanoğlu, M. Yildirim, W. Piyawattanametha, H. Ra, O. Solgaard, and A. Ben-Yakar, "Optical design and imaging performance testing of a 9.6-mm diameter femtosecond laser microsurgery probe," Opt. Express **19**(11), 10536–10552 (2011).
13. C. M. Brown, D. R. Rivera, I. Pavlova, D. G. Ouzounov, W. O. Williams, S. Mohanan, W. W. Webb, and C. Xu, "*In vivo* imaging of unstained tissues using a compact and flexible multiphoton microendoscope," J. Biomed. Opt. **17**(4), 040505 (2012).
14. D. M. Huland, C. M. Brown, S. S. Howard, D. G. Ouzounov, I. Pavlova, K. Wang, D. R. Rivera, W. W. Webb, and C. Xu, "*In vivo* imaging of unstained tissues using long gradient index lens multiphoton endoscopic systems," Biomed. Opt. Express **3**(5), 1077–1085 (2012).
15. F. Helmchen, W. Denk, and J. N. Kerr, "Miniaturization of two-photon microscopy for imaging in freely moving animals," Cold Spring Harb. Protoc. **2013**(10), 904–913 (2013).
16. S. Tang, J. Liu, T. B. Krasieva, Z. Chen, and B. J. Tromberg, "Developing compact multiphoton systems using femtosecond fiber lasers," J. Biomed. Opt. **14**(3), 030508 (2009).
17. G. Liu, K. Kieu, F. W. Wise, and Z. Chen, "Multiphoton microscopy system with a compact fiber-based femtosecond-pulse laser and handheld probe," J. Biophotonics **4**(1-2), 34–39 (2011).
18. K. Murari, Y. Zhang, S. Li, Y. Chen, M.-J. Li, and X. Li, "Compensation-free, all-fiber-optic, two-photon endomicroscopy at 1.55 μm," Opt. Lett. **36**(7), 1299–1301 (2011).
19. W. Göbel, A. Nimmerjahn, and F. Helmchen, "Distortion-free delivery of nanojoule femtosecond pulses from a Ti:sapphire laser through a hollow-core photonic crystal fiber," Opt. Lett. **29**(11), 1285–1287 (2004).
20. J. Yu, H. Zeng, H. Lui, J. S. Skibina, G. Steinmeyer, and S. Tang, "Characterization and application of chirped photonic crystal fiber in multiphoton imaging," Opt. Express **22**(9), 10366–10379 (2014).
21. W. R. Zipfel, R. M. Williams, R. Christie, A. Y. Nikitin, B. T. Hyman, and W. W. Webb, "Live tissue intrinsic emission microscopy using multiphoton-excited native fluorescence and second harmonic generation," Proc. Natl. Acad. Sci. U.S.A. **100**(12), 7075–7080 (2003).
22. J. R. Unruh, E. S. Price, R. G. Molla, L. Stehno-Bittel, C. K. Johnson, and R. Hui, "Two-photon microscopy with wavelength switchable fiber laser excitation," Opt. Express **14**(21), 9825–9831 (2006).
23. W. Chun, D. Do, and D.-G. Gweon, "Design and demonstration of multimodal optical scanning microscopy for confocal and two-photon imaging," Rev. Sci. Instrum. **84**(1), 013701 (2013).
24. D. M. Huland, M. Jain, D. G. Ouzounov, B. D. Robinson, D. S. Harya, M. M. Shevchuk, P. Singhal, C. Xu, and A. K. Tewari, "Multiphoton gradient index endoscopy for evaluation of diseased human prostatic tissue *ex vivo*," J. Biomed. Opt. **19**(11), 116011 (2014).
25. M. Hofer, M. E. Fermann, F. Haberl, M. H. Ober, and A. J. Schmidt, "Mode locking with cross-phase and self-phase modulation," Opt. Lett. **16**(7), 502–504 (1991).
26. K. Tamura, L. Nelson, H. Haus, and E. Ippen, "Soliton versus nonsoliton operation of fiber ring lasers," Appl. Phys. Lett. **64**(2), 149–151 (1994).
27. L. E. Myers, R. Eckardt, M. Fejer, R. Byer, W. Bosenberg, and J. Pierce, "Quasi-phase-matched optical parametric oscillators in bulk periodically poled $LiNbO_3$," J. Opt. Soc. Am. B **12**(11), 2102–2116 (1995).
28. G. D. Boyd and D. A. Kleinman, "Parametric Interaction of Focused Gaussian Light Beams," J. Appl. Phys. **39**(8), 3597–3639 (1968).
29. K. Moutzouris, E. Adler, F. Sotier, D. Träutlein, and A. Leitenstorfer, "Multimilliwatt ultrashort pulses continuously tunable in the visible from a compact fiber source," Opt. Lett. **31**(8), 1148–1150 (2006).
30. L. Gruner-Nielsen, M. Wandel, P. Kristensen, C. Jorgensen, L. V. Jorgensen, B. Edvold, B. Palsdottir, and D. Jakobsen, "Dispersion-compensating fibers," J. Lightwave Technol. **23**(11), 3566–3579 (2005).
31. P. C. Cheng, B. L. Lin, F. J. Kao, C. K. Sun, Y. S. Wang, T. M. Liu, Y. Wang, J. Chen, M. K. Huang, and I. Johnson, "Multiphoton fluorescence spectroscopy of flourescent bioprobes and biomolecules," Proc. SPIE **4082**, 87–91 (2000).

1. Introduction

Multiphoton microscopy (MPM) is an important tool for non-invasive and high-resolution imaging, featuring in neurology [1, 2] and cancer research [3, 4]. It utilizes femtosecond lasers to excite nonlinear contrast signals including two-photon excitation fluorescence (TPEF) and second harmonic generation (SHG) [5, 6]. TPEF can be detected from intrinsic sources and exogenous fluorophores, while strong SHG signals can be detected from noncentrosymmetric molecules such as collagen. As such, MPM is capable of imaging and distinguishing cellular and extracellular matrix structures simultaneously. The small footprint and flexibility of a compact fiber-optic MPM system using a miniaturized probe [7–15] have a great potential to transform the powerful MPM technology for *in vivo* studies and clinical applications of epithelial tissues and internal organs [7, 13–15]. However, most of the current MPM systems have a bulky overall size due to the use of a Ti:sapphire laser which is expensive, not portable, and requires precise alignment.

#259144 Received 9 Feb 2016; revised 5 Apr 2016; accepted 6 Apr 2016; published 19 Apr 2016

Currently, femtosecond fiber lasers have emerged as a promising excitation source for compact MPM systems [16–18], because they are more compact, robust, not susceptible to misalignment, and direct coupling with fiber. By using a commercial Yb-doped fiber laser, Tang *et al.* developed a compact MPM system, where a hollow core photonic bandgap fiber (PBF) was used to deliver 150 fs pulses without any dispersion compensation scheme [16]. The hollow-core PBF can nearly completely eliminate pulse broadening without prechirping at the zero-dispersion wavelength [19]; however, it can significantly broaden the output pulses above or below the exact zero-dispersion wavelength, and thus dispersion compensation is still needed when using broadband ultrashort lasers or tunable lasers [20]. A home-built Yb-doped fiber laser reported by Liu *et al.* was used in an MPM system with a handheld probe [17]. The output pulse had a pulsewidth of 125 fs and was delivered to a dispersion compensation unit which consisted of a grating pair and then coupled to a double cladding photonic crystal fiber (DCPCF). The DCPCF can deliver the excitation beam in the inner core and collects the signal with a larger cladding and thus its detection efficiency is much higher than the single mode fiber (SMF). However, DCPCF suffers severe pulse broadening and it needs to be compensated by tuning the gratings, which makes the whole system bulky and sensitive to alignment. Furthermore, since the Yb-doped fiber laser works at 1030 nm, fluorescence staining of samples is required to generate TPEF signals.

Murari *et al.* reported a fiber-optic multiphoton endomicroscopy based on a customized Er-doped fiber laser, which included a seed laser, a fiber-based pulse stretcher, an Er-doped fiber amplifier (EDFA), and a fiber-based pulse compressor [18]. The seed pulses were launched into a pulse stretcher which was a customized dispersion-shifted SMF with normal dispersion at 1.55 μm, while a standard SMF has anomalous dispersion at 1.55 μm. The stretched pulses were amplified by the EDFA and then compressed through a SMF-28 fiber. A customized double cladding fiber (DCF) was used to deliver the pulses to the endoscope probe. Since the DCF had similar dispersion and mode field diameter as the fiber compressor, it could be considered as part of the compressor. The benefit of a longer excitation wavelength is deep penetration due to considerably reduced scattering [18]. However, the disadvantages of using 1.55 μm excitation wavelength are the need of sample staining and reduced resolution [17].

Many intrinsic biological molecules have maximal two-photon excitation cross sections at shorter than 800 nm wavelength [21], thus highlighting the importance of laser sources with a central wavelength in the region of 700~800 nm for *in vivo* multiphoton imaging. Frequency doubling of commercial Er-doped fiber lasers at 780 nm have been utilized in bench-top MPM systems [22, 23]. In the reported work, the frequency-doubled commercial fiber laser had a free-space output and the fiber laser was simply utilized as a free-space source. A commercial frequency-doubled Er-doped fiber laser has been utilized in a fiber-optic MPM endoscope system [24]. The frequency-doubled output was also in free space. The free-space output was then coupled into a hollow core PBF to deliver the pulses to the endoscope. Since the pulses entered the free space and needed to be coupled into fiber again, the fiber laser lost the capability of all-fiber delivery to the distal end of the endoscope.

In this paper, we propose a miniature fiber-optic MPM probe system based on a frequency-doubled femtosecond Er-doped fiber laser. The laser is directly coupled to the probe through a SMF-28 fiber, which makes the entire system plug-and-play. A frequency-doubling crystal is mounted inside the distal end of the probe and optimized together with the laser to obtain a frequency-doubled beam with relatively high power and short pulsewidth. The frequency-doubled beam at 786 nm is used as the excitation beam to excite intrinsic MPM signals from biological samples, which eliminates the need of staining the samples. Micro-electro-mechanical system (MEMS) scanner, miniature objective, and multimode fiber are further used to make the MPM probe compact. *Ex vivo* images of mammalian skins are obtained to demonstrate the capability of the miniature fiber-optic MPM probe in imaging

#259144 Received 9 Feb 2016; revised 5 Apr 2016; accepted 6 Apr 2016; published 19 Apr 2016

biological tissues. The preliminary results demonstrate the potential of the miniature fiber-optic MPM system for clinical *in vivo* imaging.

2. System design

2.1 Er-doped fiber laser

The schematic diagram of the MPM system is shown in Fig. 1. It includes two major parts – an Er-doped fiber laser and a compact MPM probe, which are shown in the two rectangle boxes in Fig. 1, respectively. The fiber laser system comprises an Er-doped fiber oscillator mode-locked via nonlinear polarization rotation [25]. The oscillator has a net dispersion D_T of slightly negative (i.e. D_T at about −0.005 ps^2) [26]. It is driven by a laser diode chip emitting 500 mW at 980 nm. It provides 20 mW of average power at a repetition rate of 67 MHz. The oscillator delivers approximately 80 fs pulses (assuming a sech pulse) centered at 1.58 μm with a spectral full-width-half-maximum (FWHM) bandwidth of 62 nm, resulting in a time-bandwidth product of 0.6, which indicates nearly transform limited pulse. The output from the oscillator is then amplified by a bi-directional pumping setup comprises of two 980 nm laser diodes with an overall cw-power of 1 W. The output power after the amplifier is around 250 mW.

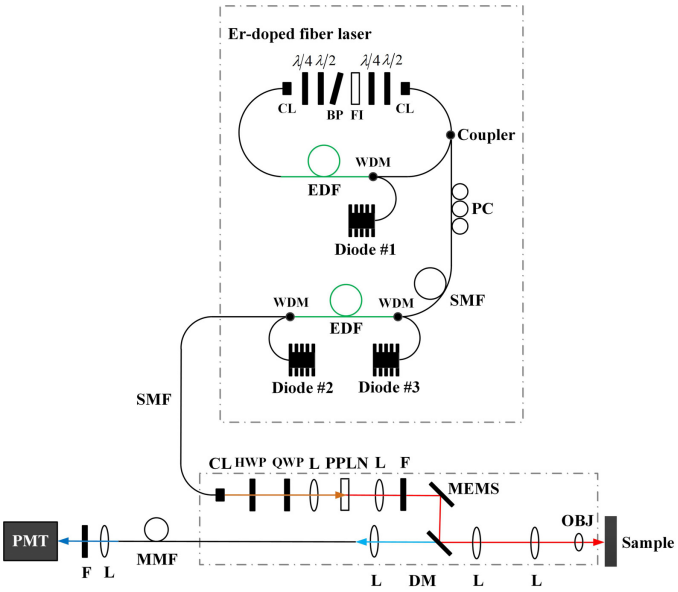

Fig. 1. Schematic the compact fiber laser based MPM system. EDF: Er-doped fiber; HWP: half-wave plate; QWP: quarter-wave plate; BP: birefringent plate; FI: faraday isolator; CL: collimating lens; WDM: wavelength division multiplexer; PC: polarization controller; SMF: single mode fiber; L: lens; PPLN: periodically poled MgO:$LiNbO_3$ crystal; F: filter; MEMS: micro-electro-mechanical scanning mirror; DM: Dichroic mirror; OBJ: objective lens; MMF: multimode fiber; PMT: photomultiplier tube.

2.2 Frequency doubling

A 110-cm-long SMF-28 fiber delivers the pulses from the Er-doped fiber laser system to the MPM probe, where the fundamental beam is frequency-doubled by a 1-mm-long periodically-poled MgO:$LiNbO_3$ (PPLN, MSHG1550-0.5-1, Covesion Ltd). A half-wave plate and a quarter-wave plate are used to maximize the power of vertically polarized fundamental beam available to be frequency-doubled by the PPLN. Maximum output power can be achieved by linearly translating the crystal to the proper grating period in order to ensure quasi-phase matching (QPM) [27]. An AR-coated focusing lens with a focal length of 7.5 mm (A375TM-

#259144 Received 9 Feb 2016; revised 5 Apr 2016; accepted 6 Apr 2016; published 19 Apr 2016

C, Thorlabs) is chosen to focus the vertically polarized fundamental pulse. This lens ensures that the ratio between the crystal length and the confocal parameter of the lens is close to 2, where the conversion efficiency is maximum [28].

The characteristics of the fundamental beam and frequency-doubled beam are shown in Fig. 2. The fundamental beam has a spectral FWHM bandwidth of nearly 8 nm in the main peak centered at 1.58 μm as shown in Fig. 2(a), and has reasonably small pulsewidth of 250 fs as shown in Fig. 2(b), albeit with satellite peaks in the autocorrelation trace. The spectrum and autocorrelation trace of the frequency-doubled pulse are shown in Figs. 2(c) and 2(d), respectively. The frequency-doubled beam has a pulsewidth of 150 fs, a central wavelength of 786 nm and a spectral FWHM bandwidth of nearly 5 nm in the main peak. With 200 mW of the amplifier output in the vertical polarization that contributes to the frequency doubling, a maximum power of 80 mW is obtained in the frequency-doubled beam, which corresponds to conversion efficiency 40%. Although the fundamental beam and frequency-doubled beam show some pulse structure and pedestals, our preliminary MPM imaging show reasonable signal-to-noise ratio (SNR). Further improvement on SNR can be achieved by eliminating the pulse structure and pedestals by using custom fibers for dispersion compensation, which will be investigated in our future study.

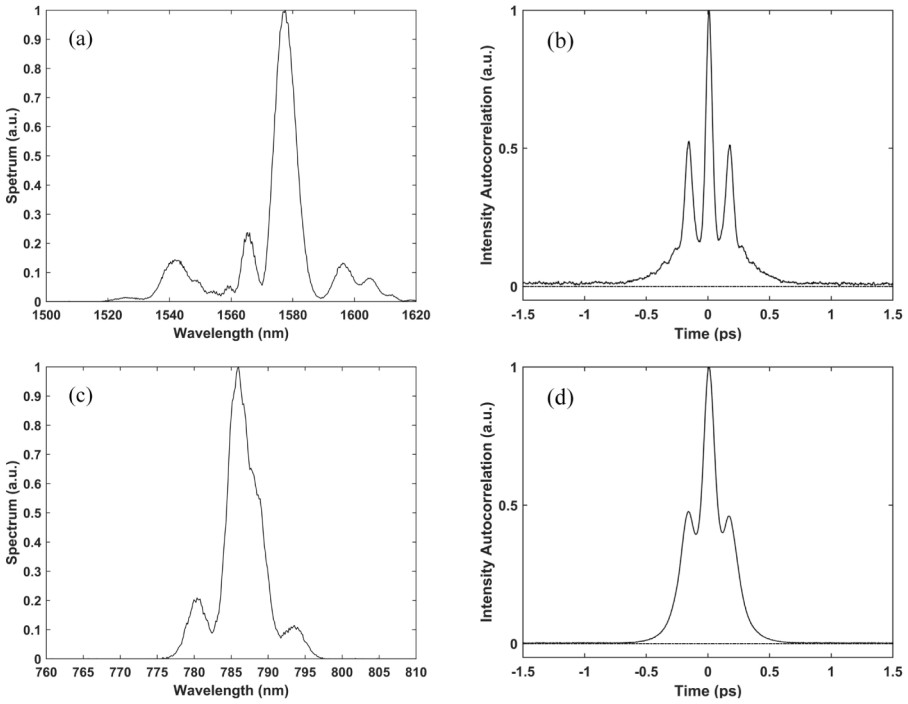

Fig. 2. Spectra of the (a) fundamental and the (c) frequency-doubled pulse and their corresponding autocorrelation traces in (b) and (d).

An important consideration in frequency doubling is the acceptance bandwidth of the nonlinear crystal. If the fundamental pulse has excessively larger spectral bandwidth than the acceptance bandwidth, the energy outside of the acceptance bandwidth will not convert to the frequency-doubled pulse. Theoretically the maximum bandwidth of the frequency-doubled beam is approximately half of the acceptance bandwidth of the PPLN [29]. The acceptance bandwidth of the 1-mm-long PPLN is 13 nm when the fundamental wavelength is 1.58 μm and it increases when the crystal length reduces. Therefore, a broader bandwidth (thus relatively a shorter pulsewidth) of the frequency-doubled beam can be achieved by the use of a shorter PPLN crystal and a fundamental beam with a bandwidth close to the corresponding

#259144 Received 9 Feb 2016; revised 5 Apr 2016; accepted 6 Apr 2016; published 19 Apr 2016

acceptance bandwidth. For example, a 0.3-mm-long PPLN has an acceptance bandwidth of about 44 nm when the fundamental wavelength is 1.58 μm. If the bandwidth of the fundamental beam can be increased to 44 nm, we can obtain shorter frequency-doubled pulses by using the 0.3-mm-long PPLN compared to the 1-mm-long crystal. Shorter pulses can potentially increase the efficiency of MPM which is inversely proportional to the pulsewidth of the excitation beam. Meanwhile, the conversion efficiency may reduce when the crystal length is shortened. Thus optimization of the MPM system will consider the fiber laser bandwidth, the PPLN thickness, the pulsewidth and power at the sample location etc., which will be a topic for future study.

In our system, the femtosecond pulses are delivered to the distal end of the probe at the 1.58 μm wavelength by the standard SMF and the frequency-doubling to 786 nm is performed inside the probe. Delivering femtosecond pulses at 1.58 μm has several advantages. First, the absolute value of group velocity dispersion (GVD) is much lower at 1.58 μm than at 786 nm in SMF. Second, standard SMF has anomalous dispersion at 1.58 μm which can be used for fiber-based dispersion compensation. Thus the pulsewidth can be minimized by adjusting the length of the output SMF to compensate for the normal dispersion from the Er-doped fiber. Furthermore, at 1.58 μm wavelength band, there are various types of dispersion compensation fibers [30] available that can precisely manage both the GVD and its slope for optimum dispersion compensation. Therefore, with our approach, we can achieve all-fiber-based dispersion compensation and also be able to operate the system at 786 nm to excite intrinsic MPM signals without the need of staining.

2.3 Miniature fiber-optic MPM probe design

The schematic of the MPM probe is indicated in the bottom rectangle box in Fig. 1, and a photograph of the assembled probe is shown in Fig. 3. After the PPLN, an aspheric lens (C220TMD-B, Thorlabs) is used to collimate the frequency-doubled beam and a glass filter (Schott RG9) is used to block the residual fundamental beam. The beam is then directed to a MEMS 2D scanner (Mirrocle Tech., Inc.) to perform raster scanning. Two identical Ø1/2" achromatic doublets (AC127-019-A, f = 19.0 mm, Thorlabs) are used to relay the beam to a miniature objective lens, where the beam fills its entire back aperture. An aspheric lens C150TME-A (f = 2.0 mm, NA = 0.50, Thorlabs) is used as the objective lens. The emitted multiphoton signals are separated from the back-reflected excitation light by a short-pass dichroic mirror (FF670-SDi01, Semrock). The signals are collected by a multimode fiber (MMF) patch cable (Ø1500 μm, NA = 0.39, Thorlabs) and sent to a PMT (H9305-03, Hamamatsu), followed by a photon counting unit (C9744, Hamamatsu). A blocking filter with a passband from 350 to 650 nm (FF01-680/SP-25, Semrock) is placed in front of the PMT in order to remove the residual of the back-reflected excitation light. The field of view of the probe is 151 μm × 236 μm (512 × 512 pixels) and the maximum power from the probe is 50 mW. The frame rate is 0.4 frames/s when the pixel dwell time is 10 μs. While the slow Y-axis of the MEMS scanner is driven by a sawtooth waveform, the fast X-axis is driven by a sinusoidal waveform to maximize its speed. Image distortion due to the sinusoidal scanning is corrected by data processing, resulting in different final image size in X and Y axis. The housing of the compact probe is made by 3D printing technology and the overall size of the packaged probe is 40 mm (height) × 45 mm (width) × 165 mm (length).

#259144 Received 9 Feb 2016; revised 5 Apr 2016; accepted 6 Apr 2016; published 19 Apr 2016

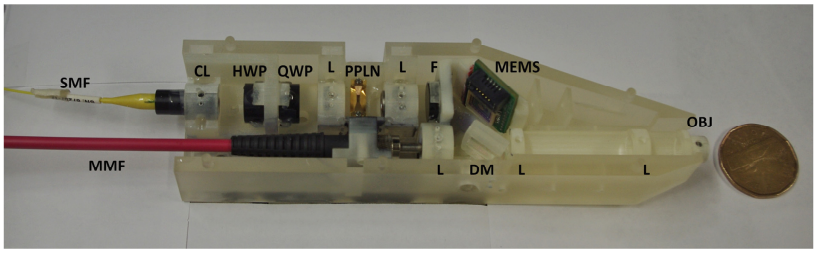

Fig. 3. A photograph of the miniature fiber-optic MPM probe. SMF: single mode fiber; CL: collimating lens; HWP: half-wave plate; QWP: quarter-wave plate; L: lens; PPLN: periodically poled MgO:$LiNbO_3$ crystal; F: filter; MEMS: micro-electro-mechanical scanning mirror; DM: Dichroic mirror; OBJ: objective; MMF: multimode fiber. The Loonie shown has a diameter of 26.5 mm.

3. Results and discussion

While the PPLN is used for frequency doubling, it also produces third harmonic generation (THG) output. The THG output of PPLN is centered at 530 nm as shown in Fig. 4. Thus the THG output of the PPLN can overlap with the TPEF signal from the sample. Generally, the TPEF signal of NADH, which is a typical native biological fluorophore, peaks around 450 nm and extends to 600 nm [31]. Thus the THG output of the PPLN can potentially reduce the SNR in the MPM system. The glass filter (Schott RG9) can block the THG output in the main beam path. However, in our study, we have observed that scattered THG output could still reach the collection fiber from the side. To reduce the effect of the THG output, the side walls of the MPM probe need to be fully blocked. Using highly opaque materials in 3D printing can block it from entering into the collection fiber.

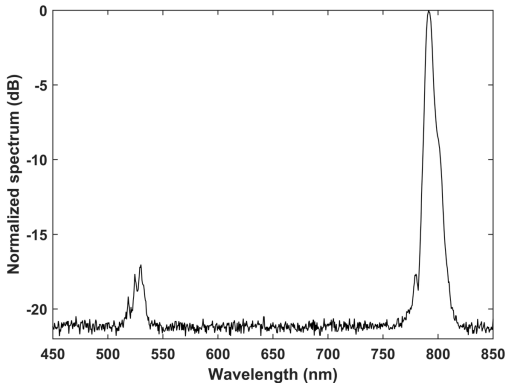

Fig. 4. The normalized spectrum of the second order generation signal and third order generation signal of PPLN.

The lateral resolution of the miniature fiber-optic MPM system is quantified by investigating the two-photon point spread function (PSF) of the 0.1-μm-diameter fluorescent beads (Fluoresbrite® Calibration Grade Size Range Kit, Polysciences, Inc.). The intensity measured across a single bead and its Gaussian fitting curve are shown in Fig. 5. The FWHM of the two-photon PSF is about 1.3 μm, which corresponds to the lateral resolution of the MPM system.

#259144 Received 9 Feb 2016; revised 5 Apr 2016; accepted 6 Apr 2016; published 19 Apr 2016

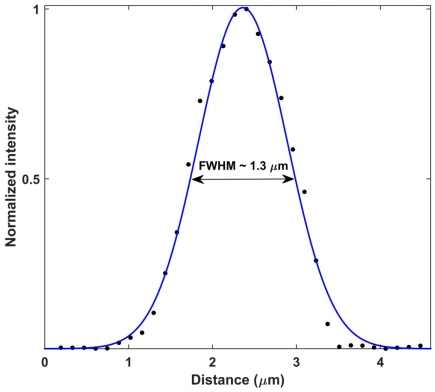

Fig. 5. The lateral two-photon PSF plot for a 0.1-μm-diameter fluorescent bead. Experimental data (black dots) and results of the Gaussian fit (in blue) are shown.

The miniature fiber-optic MPM system is applied to image several biological tissue samples. The tissues are kept in saline and imaged within two hours postmortem. The power on sample is ~50 mW. The SHG image of a skin sample from a Yucatan pig is shown in Fig. 6(a), and the SHG image of a skin sample from a Zealand white rabbit is shown in Fig. 6(b). These SHG images show clear collagen structures in the dermal layer. The collagen fiber structures seem to be finer in the rabbit skin than in the pig skin. The TPEF image of a skin sample from a CD-1 mouse is shown in Fig. 6(c), in which the cells in the epidermal layer are observed. The intrinsic TPEF signals are observed to be much weaker than the SHG signals in our samples and Fig. 6(c) is averaged over 10 frames. For all the images, the pixel dwell time is 10 μs and the image size is 151 μm × 236 μm. All these *ex vivo* images are staining-free, showing that the miniature fiber-optic MPM probe system has the capability of imaging intrinsic signals from biological tissues. The current imaging speed is limited by the relatively low SNR. Increasing the system SNR is possible by optimizing the fiber laser and the frequency doubling process to achieve shorter pulses, and designing a compound miniature objective to focus the laser beam into a smaller focal volume on the sample. Such investigations will be carried out in our future study.

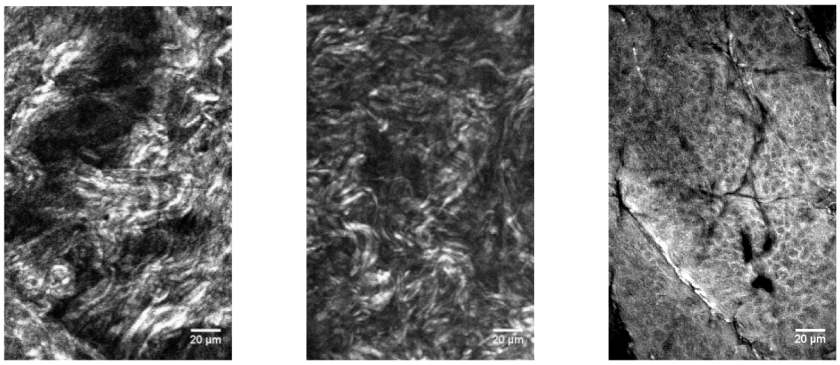

(a) (b) (c)

Fig. 6. Images acquired by the miniature fiber-optic MPM probe system. (a) SHG image of a porcine skin. (b) SHG image of a leporine skin. (c) TPEF image of a murine skin averaged over 10 frames. Scale bar is 20 μm.

4. Conclusions

In summary, we have developed a miniature fiber-optic MPM system based on frequency-doubled femtosecond Er-doped fiber laser. The laser is directly coupled to the MPM probe

#259144 Received 9 Feb 2016; revised 5 Apr 2016; accepted 6 Apr 2016; published 19 Apr 2016

through a SMF-28 fiber and the emitted signals are collected through a MMF patch cable, making the whole setup fiber connected. The miniature fiber-optic MPM system is compact, portable, and robust. *Ex vivo* SHG/TPEF images of unstained skin samples are acquired to verify the imaging capability of the miniature fiber-optic MPM system. With the compact femtosecond fiber laser and the MPM probe, *in vivo* imaging will become possible and different locations in the samples can become easier to be accessed.

Acknowledgments

This work is supported by the Natural Sciences and Engineering Research Council, the BCFRST Foundation, and the British Columbia Innovation Council of Canada. The authors wish to thank Dr. Shaupoh Chong for his initial design of the laser.

#259144 Received 9 Feb 2016; revised 5 Apr 2016; accepted 6 Apr 2016; published 19 Apr 2016